Journal of the Optical Society of America B
OPTICAL PHYSICS

Effective terahertz signal detection via electromagnetically induced transparency in graphene

SHAOPENG LIU,[1] WEN-XING YANG,[1,2,*] ZHONGHU ZHU,[1] AND RAY-KUANG LEE[2]

[1]Department of Physics, Southeast University, Nanjing 210096, China
[2]Institute of Photonics Technologies, National Tsing-Hua University, Hsinchu 300, Taiwan
*Corresponding author: wenxingyang2@126.com

Received 27 October 2015; revised 8 December 2015; accepted 19 December 2015; posted 22 December 2015 (Doc. ID 252664); published 1 February 2016

We propose and analyze an efficient way to detect the terahertz (THz) signal in a magnetized graphene system via electromagnetically induced transparency. Such a scheme for THz signal detection mainly relies on the measurement of probe transmission spectra, in which the behaviors of a weak-probe transmission spectra can be controlled by switching on/off the THz signal radiation. Taking into account the tunable optical transition frequency between the Landau levels in graphene, our analytical results demonstrate that a broad frequency bandwidth of the THz signal radiation, ranging from 0.36 to 11.4 THz, can be inspected and modulated by means of an external magnetic field. As a consequence, the proposed magnetized graphene system performs a striking potential to utilize quantum interference in the design of optical solid-state devices.

OCIS codes: (270.1670) Coherent optical effects; (040.2235) Far infrared or terahertz.

http://dx.doi.org/10.1364/JOSAB.33.000279

1. INTRODUCTION

Graphene, consisting of a series of carbon atoms in the two-dimensional hexagonal lattice, has attracted considerable scientific interest in its fascinating electronic and optical properties during the past few years. These electronic properties originating from linear, massless dispersion of electrons near the Dirac point and the chiral character of electron states have motivated a number of recent theoretical investigations in graphene [1–3]. The magneto-optical properties and thin graphite layers give rise to multiple absorption peaks and particular selection rules between Landau levels (LLs) [4–7]. Subsequently, due to its unusual band structure and selection rules for the optical transitions, an intriguing optical nonlinearity in the infrared (IR) and terahertz (THz) region [5,6,8–13] has been exploited in the wide applications. For example, Yao *et al.* have calculated the THz radiation power generated by the four-wave mixing and stimulated Raman scattering processes in graphene [10]. In addition, several quantum theories about the frequency mixing effects and infrared solitons in graphene have been developed [14–17]. From the viewpoint of practical applications, graphene may provide a better access to the characterization and manipulation of optical properties in the THz region.

On the other hand, quantum interference in the form of electromagnetically induced transparency (EIT) has led to many significant research activities on optical communications and quantum information processing in both cold atom media and semiconductors [18–22]. This concept of quantum interference has also been extended to a variety of studies, such as controlling the group velocity of light pulses [23,24], optical solitons [25,26], multiwave mixing process [27–29], optical bistability [30], and THz signal detection strategy [31–35]. In particular, the THz science is expected to have a wide range of applications in diverse fields, including biological imaging, long-distance detection of hazardous materials, and nondestructive testing [36–38]. Inspired by the linear and nonlinear optical response of graphene in the IR and THz regions, we suggest a scheme for detecting and measuring the THz signal radiation by using EIT in graphene, which may open up an avenue to explore new availability for creating a compact and inexpensive THz detector.

In this paper, we study a novel optical method to detect the THz signal based on EIT in a quantized three-level graphene system under a strong magnetic field. Different from the most common THz technique using nonlinear multiplication or up-conversion of lower-frequency oscillators [39,40], our scheme based on quantum interference associating with one weak mid-infrared probe light is analyzed for achieving the THz signal detection. Under suitable conditions, a strong absorption characteristic of the probe field appears in the absence of the THz signal, while the optical absorption of the probe field can be

absolutely suppressed with the THz signal switched on. The different response depends, respectively, on whether quantum destructive interference is quenched or well developed so that we can examine the existence of the EIT transparency window and THz signal field. In addition, a time-dependent analysis performs the probe pulse propagating with an ultraslow group velocity (i.e., $V_g \simeq 10^{-3} \sim 10^{-4}c$) at a low-intensity domain. Motivated by establishing a practical and effective approach, the transmission spectra of the probe field is finally simulated by employing the incident Gaussian-shaped probe pulse in our scheme of THz signal detection.

2. THEORETICAL MODEL AND BASIC EQUATIONS

In this section, we propose a 2D graphene crystal structure with three energy levels in the presence of a strong magnetic field, as shown in Figs. 1(a)–1(c). Because of the special selection rules in present graphene, the selected transitions are dipole allowed between the appointed energy levels, i.e., $\Delta|n| = \pm 1$ (n is the energy quantum number). Specially, the right-hand circularly (RHC) polarized photons could be homogeneously applied to the condition of $\Delta|n| = -1$, and the left-hand circularly (LHC) polarized photons are simultaneously applied to the case of $\Delta|n| = +1$ [5]. The application of the external magnetic field results in the formation of discrete LLs, as shown in Fig. 1(b). It should be noted that the carrier frequencies of optical transition between adjacent LLs turn out to be in the IR or THz region for a magnetic field in the range of 0.01–10 T: $\hbar\omega_c \simeq 36\sqrt{B(\text{Tesla})}$ meV [6,10,41] (see Appendix A). We consider the electric field vector of the system that can be expressed as $\vec{E}_p = \vec{e}_- E_p^- \exp(-i\omega_p t + i\vec{k}_p \cdot \vec{r}) + \text{c.c.}$ and $\vec{E}_{TH} = \vec{e}_- E_{TH}^- \exp(-i\omega_{TH} t + i\vec{k}_{TH} \cdot \vec{r}) + \text{c.c.}$, where $\vec{e}_-(\vec{e}_+)$ corresponds to the unit vector of the LHC (RHC) polarized basis, which can be noted as $\vec{e}_- = [\hat{x} - i\hat{y}]/\sqrt{2}(\vec{e}_+ = [\hat{x} + i\hat{y}]/\sqrt{2})$. In detail, the optical field of the LHC polarized component E_p^- (E_{TH}^-) with the carrier frequency ω_p (ω_{TH}) constructs the optical transition $|1\rangle \leftrightarrow |2\rangle$ ($|2\rangle \leftrightarrow |3\rangle$), respectively.

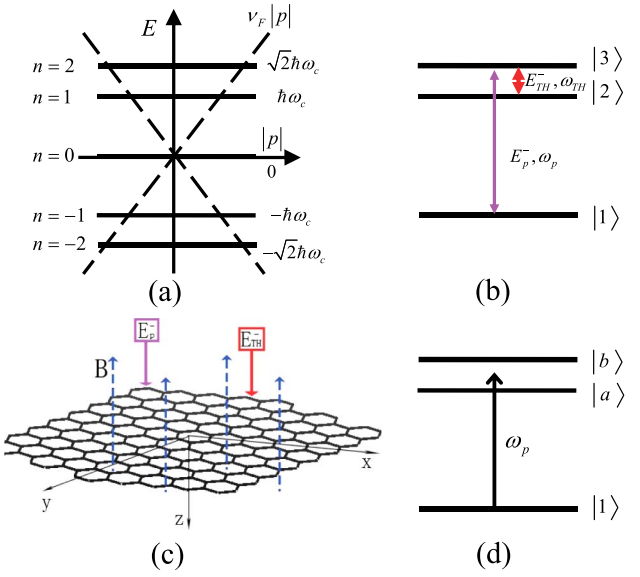

Fig. 1. (a) Landau levels (LLs) near the Dirac point superimposed on the linear electron dispersion without the magnetic field $E = \pm v_F|p|$. The magnetic field condenses the original states in the Dirac cone into discrete energies. (b) Energy level diagram and optical transitions in graphene interacting with a weak probe pulse (with carrier frequency ω_p) and a THz signal field (with carrier frequency ω_{TH}). The states $|1\rangle$, $|2\rangle$, and $|3\rangle$ correspond to the LLs with energy quantum numbers $n = -1, 1, 2$, respectively. (c) Geometry of the system. The probe pulse and THz signal field are perpendicularly incident on the single-layer graphene (the monolayer graphene is regarded as a perfect two-dimensional (2D) crystal structure in the $x - y$ plane) placed in a magnetic field B, in which both two optical fields and magnetic field are along the z-axis. (d) Schematic of the two dressed states $|a\rangle$ and $|b\rangle$ produced by states $|2\rangle$ and $|3\rangle$ coupled with state $|1\rangle$ in the presence of the THz signal.

When the magnetic field is perpendicularly applied in a single-layer graphene (in the $x - y$ plane), the optical transitions driven by the probe pulse and THz signal field generate the quantum interference and quantum coherence effects. In the interaction picture, with the rotating wave approximation and the electric dipole approximation (see Appendix A), the total Hamiltonian of this system can be written as

$$\hat{H}_{\text{int}}^I = \Delta_p|3\rangle\langle 3| + (\Delta_p - \Delta_{TH})|2\rangle\langle 2| - (\Omega_p|3\rangle\langle 1| + \Omega_{TH}|3\rangle\langle 2| + \text{h.c.}), \quad (1)$$

where the corresponding frequency detunings are given by $\Delta_p = (\varepsilon_{n=2} - \varepsilon_{n=-1})/\hbar - \omega_p$ and $\Delta_{TH} = (\varepsilon_{n=2} - \varepsilon_{n=1})/\hbar - \omega_{TH}$. The energy of the LLs for electrons near the Dirac point is denoted as $\varepsilon_n = \text{sgn}(n)\hbar\omega_c\sqrt{|n|}(n = 0, \pm 1, \pm 2)$ with $\omega_c = \sqrt{2}v_F/l_c$ and $l_c = \sqrt{\hbar c/eB}$ representing the magnetic length. The corresponding Rabi frequencies for the relevant laser-driven intersubband transitions are represented as $\Omega_p = (\vec{\mu}_{31} \cdot \vec{e}_-)E_p^-/\hbar$ and $\Omega_{TH} = (\vec{\mu}_{32} \cdot \vec{e}_-)E_{TH}^-/\hbar$, in which $\vec{\mu}_{mn} = \langle m|\vec{\mu}|n\rangle = e \cdot \langle m|\vec{r}|n\rangle = \frac{i\hbar e}{\varepsilon_n - \varepsilon_m}\langle m|v_F\vec{\sigma}|n\rangle$ denotes the dipole moments for the transition between states $|m\rangle \leftrightarrow |n\rangle$.

In the present analysis, to obtain the absorption-dispersion properties of the graphene system, we first adopt Liouville's equation $\frac{\partial\hat{\rho}}{\partial t} = -\frac{i}{\hbar}[\hat{H}_{\text{int}}^I, \hat{\rho}] - \hat{R}(\hat{\rho})$. Here, $\hat{R}(\hat{\rho}) = \frac{1}{2}\{\hat{\Gamma}, \hat{\rho}\} = \frac{1}{2}\{\hat{\Gamma}\hat{\rho} + \hat{\rho}\hat{\Gamma}\}$ indicates incoherent relaxation, which may stem from disorder, interaction with phonons and carrier–carrier interactions. Moreover, the decay rate of the graphene is combined into the evolution equation by a relaxation matrix $\hat{\Gamma}$, which can be defined by $\langle n|\hat{\Gamma}|m\rangle = \gamma_n\delta_{nm}$. Subsequently, a standard time-evolution equation for the density matrix of Dirac electrons in graphene coupled to the infrared laser fields can be calculated as follows,

$$\begin{aligned}
\dot{\rho}_{11} &= i\Omega_p^*\rho_{31} - i\Omega_p\rho_{13}, \\
\dot{\rho}_{22} &= -\gamma_2\rho_{22} + i\Omega_{TH}\rho_{32} - i\Omega_{TH}^*\rho_{23}, \\
\dot{\rho}_{33} &= -\gamma_3\rho_{33} + i\Omega_p\rho_{13} - i\Omega_p^*\rho_{31} + i\Omega_{TH}^*\rho_{23} - i\Omega_{TH}\rho_{32}, \\
\dot{\rho}_{31} &= -\left(\frac{\gamma_3}{2} + i\Delta_p\right)\rho_{31} + i\Omega_p(\rho_{11} - \rho_{33}) + i\Omega_{TH}\rho_{21}, \\
\dot{\rho}_{21} &= -\left(\frac{\gamma_2}{2} + i(\Delta_p - \Delta_{TH})\right)\rho_{21} + i\Omega_{TH}^*\rho_{31} - i\Omega_p\rho_{23}, \\
\dot{\rho}_{32} &= -\left(\frac{\gamma_3 + \gamma_2}{2} + i\Delta_{TH}\right)\rho_{32} + i\Omega_{TH}(\rho_{22} - \rho_{33}) + i\Omega_p\rho_{12},
\end{aligned} \quad (2)$$

where $\gamma_i (i = 2, 3)$ corresponds to the decay rate of states $|i\rangle$. And the steady-state solutions for Eq. (2) can be derived as

$$\rho_{21} = \frac{-\Omega_p \Omega_{TH}}{\Omega_{TH}^2 + d_{21} d_{31}}, \qquad \rho_{31} = \frac{-i d_{21} \Omega_p}{\Omega_{TH}^2 + d_{21} d_{31}}, \tag{3}$$

with $d_{21} = -[\frac{\gamma_2}{2} + i(\Delta_p - \Delta_{TH})]$, $d_{31} = -(\frac{\gamma_3}{2} + i\Delta_p)$.

Under an appropriate frame, we can substitute straightforwardly results of Eq. (3) into the slowly varying parts of the polarization of the weak probe pulse, i.e., $P = \varepsilon_0 \chi(\omega_p) E_p = N(\mu_{31}\rho_{31} + \text{c.c.})$, with N being the electron concentration. The expression for the susceptibility $\chi(\omega_p)$ can therefore be written as

$$\chi(\omega_p) = \frac{N\mu_{31}^2}{\varepsilon_0 \hbar} \cdot \frac{\rho_{31}}{\Omega_p} = \beta \frac{-i d_{21}}{d_{21} d_{31} + \Omega_{TH}^2}, \tag{4}$$

where the parameter β is noted as $\beta = N\mu_{31}^2/\varepsilon_0 \hbar$. The real and imaginary parts of susceptibility $\chi(\omega_p)$ are still linear with respect to dispersion and absorption of the graphene system, respectively. Further, the absorption coefficient for the probe field coupled to $|1\rangle \leftrightarrow |3\rangle$ is directly proportional to the imaginary part of $\text{Im}(\rho_{31})$, while the transmission coefficient of the probe field is spontaneously proportional to the imaginary part of susceptibility. For the propagation effect of the probe field, the electronic equations of motion must be simultaneously solved with Maxwell's equation in a self-consistent manner. Under the condition of slowly varying envelope approximation, Rabi frequency Ω_p of the probe field is governed by the following Maxwell's equation,

$$\frac{\partial \Omega_p}{\partial z} + \frac{1}{v_F} \frac{\partial \Omega_p}{\partial t} = i\alpha_p \gamma_3 \rho_{31}, \tag{5}$$

where the parameter $\alpha_p = \frac{N\omega_p |\mu_{31}|^2}{4\hbar \varepsilon_r v_F \gamma_3}$ is the propagation constant of the probe field. When Ω_p^{in} is assumed as the initial probe field at the entrance $z = 0$, we arrive at the linearized results for propagation dynamics of the probe field at the output $z = L$:

$$\Omega_p^{\text{out}} = \Omega_p^{\text{in}} e^{-\alpha_p L \gamma_3 \text{Im}\left(\frac{\rho_{31}}{\Omega_p}\right)}. \tag{6}$$

Based on Eqs. (4)–(6), the normalized transmission coefficient of the probe field has the form $T \equiv \Omega_p^{\text{out}}/\Omega_p^{\text{in}}$.

It should be pointed out that the carrier frequencies of relevant LLs can be estimated by an amount of the transition frequencies $\omega_{31} = (\varepsilon_{n=2} - \varepsilon_{n=-1})/\hbar = (\sqrt{2} + 1)\omega_c$ and $\omega_{32} = (\varepsilon_{n=2} - \varepsilon_{n=1})/\hbar = (\sqrt{2} - 1)\omega_c$, and the carrier frequency ω_c is determined by the magnetic field B. For the magnetic field up to 3 T, transition frequency ω_c is of the order of $\omega_c \simeq 10^{14}$ s^{-1}. In this scenario, $\nu_{31} \simeq 38.4$ THz (i.e., $\omega_{31} \simeq 2.41 \times 10^{14}$ s^{-1}) is located within the mid-infrared region, while the $\nu_{32} \simeq 6.59$ THz (i.e., $\omega_{32} \simeq 4.14 \times 10^{13}$ s^{-1}) belongs to the THz region. According to the numerical estimate based on [6,41], the decay rates can be estimated to be $\gamma_3 = 3 \times 10^{13}$ s^{-1} and $\gamma_2 = 0.05\gamma_3$. For the present graphene system, the dipole moment between the transition $|1\rangle \leftrightarrow |3\rangle$ has a magnitude of the order of $|\vec{\mu}_{31}| \sim \hbar e v_F/(\varepsilon_{n=2} - \varepsilon_{n=-1}) \propto 1/\sqrt{B}$. The electron concentration can be estimated to be $N \simeq 5 \times 10^{12}$ cm^{-2} and the substrate dielectric constant turns out to be $\varepsilon_r \simeq 4.5$ [42–44]. These parameter values rely on the sample quality and the substrate used in the experiment [6,9,10,45,46].

3. NUMERICAL RESULTS AND DISCUSSION

It is well known that the frequencies involved in the optical transitions between adjacent LLs fall into the IR and THz region in the magnetized graphene and have a sensitive dependent on the strength of the magnetic field via the relation $\hbar\omega_c \simeq 36\sqrt{B(\text{Tesla})}$. Within the above practical parameter set, we plot the transmission spectra of the probe field as a function of the probe frequency and the magnetic field without and with including the THz signal field, as shown in Fig. 2. For the two cases, we investigate the transmission spectra of the probe field in the external magnetic field ranging from 0.01 to 10 T. When the THz signal radiation is off (i.e., $|\Omega_{TH}| = 0$) in Fig. 2(a), one can see that the only high absorption line appears in the center of the probe transmission spectra. And the center frequency of the probe absorption peak has a shift in the mid-infrared region with the increase of the magnetic field. When the THz signal opens in Fig. 2(b), the original high absorption line becomes an obvious transparency window between two high absorption lines. Thus, the THz signal radiation can be regarded as a switch to manipulate the probe transmission spectra with absorption or transparency.

In order to simplify the above physical picture, in Fig. 3(a) we show the transmission spectra of the probe fields versus the probe frequency, while keeping the external magnetic field fixed

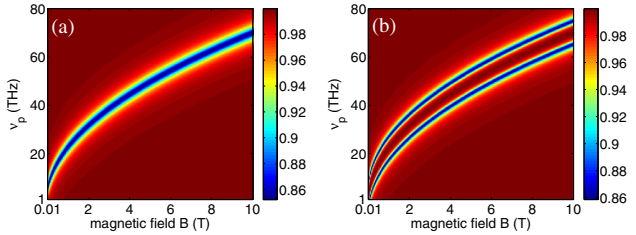

Fig. 2. Contour maps of transmission spectra of the probe field as a function of the probe frequency and the magnetic field. (a) Without including THz signal, $|\Omega_{TH}| = 0$; (b) with including THz signal, $|\Omega_{TH}| = \gamma$. Other parameters are $\Delta_{TH} = 0$, $\gamma = 3 \times 10^{13}$ s^{-1}, $\gamma_3 = \gamma$, $\gamma_2 = 0.05\gamma_3$, $|\Omega_p| = 0.05\gamma$, $L = 0.4$ nm, and $\alpha_p = 200$ μm^{-1}.

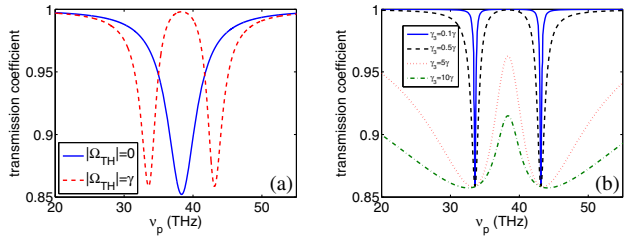

Fig. 3. (a) Transmission spectra of the probe field versus probe frequency for different THz signals with $\gamma_3 = \gamma$. (b) Transmission spectra of the probe field versus probe frequency for different losses of graphene with $|\Omega_{TH}| = \gamma$. Other parameters are $B = 3T$, $\Delta_{TH} = 0$, $\gamma = 3 \times 10^{13}$ s^{-1}, $\gamma_2 = 0.05\gamma_3$, $|\Omega_p| = 0.05\gamma$, $L = 0.4$ nm, and $\alpha_p = 200$ μm^{-1}.

(i.e., $B = 3T$). In the probe transmission spectra of the magnetized graphene system, a low transmission valley or high absorption peak appears around the resonant probe frequency (i.e., $\nu_p = \omega_{31}/2\pi = 38.42$ THz) when the THz signal field switches off (i.e., $|\Omega_{TH}| = 0$). Contrarily, the narrow EIT transparency window can be observed by switching on the THz signal radiation (i.e., $|\Omega_{TH}| = \gamma$). In fact, these different optical responses depend significantly on whether quantum destructive interference is quenched or well developed [19,47,48] by modifying the strength of THz signal radiation. To investigate the influence of losses in graphene, we plot the probe transmission spectra versus probe frequency for different losses of graphene; see Fig. 3(b). The influence of losses in graphene is mainly embodied in the transparency extent of the EIT window, while keeping the optical laser fields fixed. That is, with the loss decreasing, the transparency window is more obvious, which strongly supports our THz detection scheme. However, the large loss of graphene leads to an intensive disturbance for the EIT transparency window. As a result, a high-quality graphene with a weak loss may provide a practical help to create the perfect transparency window. Furthermore, the above physical phenomenon can be also explained by dressed states theory. Here, to achieve better EIT phenomenon, we assume that the probe pulse and THz signal field satisfy the resonance condition (i.e., $\Delta_p = 0$ and $\Delta_{TH} = 0$) and the relation $|\Omega_{TH}| \gg |\Omega_p|$. Simultaneously, the excited subband $|3\rangle$ is coupled by the probe pulse to the ground state with μ_{31}, while it is intensively coupled by the THz signal field to the subband $|2\rangle$ with μ_{32}. There are two dress states $|a\rangle$ and $|b\rangle$, as shown in Fig. 1(d). The corresponding dress states under the one-photon resonance condition can be expressed as

$$|a\rangle = \frac{1}{\sqrt{2}}(|3\rangle + |2\rangle), \qquad |b\rangle = \frac{1}{\sqrt{2}}(|3\rangle - |2\rangle), \tag{7}$$

with the energy eigenvalues of the two dressed states $\lambda_{a,b} = \pm\Omega_{TH}$. When the frequency detuning of the probe field is tuned at $\Delta_p = \lambda_a$ and $\Delta_p = \lambda_b$, two resonant excitations happen through the channels in the dressed state basis $|1\rangle \to |a\rangle$ and $|1\rangle \to |b\rangle$, which correspond to the two absorption peaks. At the position of probe resonance $\Delta_p = 0$, the superposition of two absorption paths creates the EIT transparency window.

According to the above result, we have verified that the different optical response of the graphene occurs at the transparency window, so that we can detect the THz signal by measuring the strength of the probe transmission spectra. In the following discussion, we mainly investigate the optical properties of the probe and THz signal fields in the magnetized graphene. First of all, we display transmission spectra of the probe field versus the THz signal intensity in Fig. 4(a). It can be seen that the transmission ratio increases monotonically with the increase of THz signal intensity until the appearance of the perfect EIT window. In comparison with the different losses of graphene, the smaller the loss of graphene is, the less THz signal intensity the perfect EIT system needs. For example, to achieve the perfect EIT window, the THz signal intensity needs to reach at least 10^5 W/cm^2 $\sim 6.25 \times 10^{23}$ photons/s per cm^2 with the loss of graphene $\gamma_3 = \gamma$, while the THz signal intensity is 10^3 W/cm^2 $\sim 6.25 \times 10^{21}$ photons/s per cm^2 with the loss $\gamma_3 = 0.1\gamma$. That is to say, we can get a further reduced THz signal intensity to achieve the perfect EIT transparency window and the THz detection scheme by decreasing the losses of the magnetized graphene system. Second, we plot the group velocity as a function of THz signal amplitude $|\Omega_{TH}|$. The group velocity of the probe field exhibits a ultraslow propagation regime and its order of magnitude reaches at 10^{-3}–10^{-4} c for the different losses of graphene. As a matter of fact, quantum destructive interference driven by the THz signal field modifies the dispersive property of graphene, leading to the slow group velocity. In view of a controllable normal dispersion property in the narrow EIT window [24], a further reduced group velocity can be obtained by choosing the related parameter values appropriately.

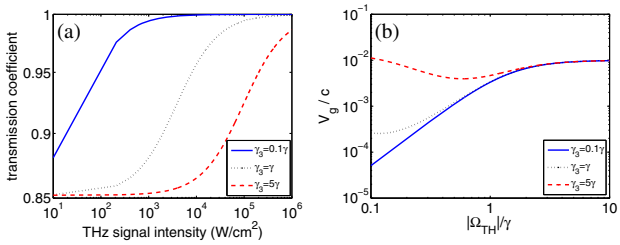

Fig. 4. (a) Transmission spectra of the probe field versus the THz signal intensity for different losses of graphene on a log–log scale. (b) Group velocity of probe light as a function of amplitude $|\Omega_{TH}|$ of THz signal field on a log–log scale. Other parameters are $B = 3T$, $\Delta_p = 0$, $\Delta_{TH} = 0$, $\gamma = 3 \times 10^{13}$ s^{-1}, $\gamma_2 = 0.05\gamma_3$, $|\Omega_p| = 0.05\gamma$, $L = 0.4$ nm, and $\alpha_p = 200$ μm^{-1}.

For a direct insight into the effect of the THz signal frequency on the probe transmission spectra, we plot the contour maps of the probe transmission spectra as a function of the THz signal frequency and the magnetic field in Fig. 5. Here, we first assume that the probe field detuning is always zero. When the THz signal frequency approaches to resonant transition frequency (i.e., $\nu_{TH} = \nu_{32} = \omega_{32}/2\pi$), the EIT window is expected to appear, so that the probe field safely passes through the graphene system. On the other hand, as the magnetic field is varying from 0.01 to 10 T, the carrier frequency ν_{32} falls into the THz region ranging from 0.36 to 11.4 THz. According to that, Fig. 5 implies that a broad bandwidth of the THz signal frequency can be accurately inspected by controlling the external magnetic field. Interestingly enough, direct comparison of

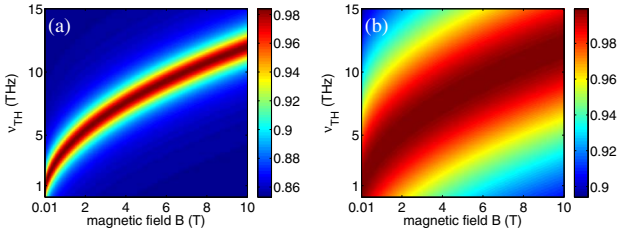

Fig. 5. Contour maps of transmission spectra of the probe field as a function of the THz signal frequency and the magnetic field. (a) $|\Omega_{TH}| = \gamma/3$; (b) $|\Omega_{TH}| = \gamma$. Other parameters are $\Delta_p = 0$, $\gamma = 3 \times 10^{13}$ s^{-1}, $\gamma_3 = \gamma$, $\gamma_2 = 0.05\gamma_3$, $|\Omega_p| = 0.05\gamma$, $L = 0.4$ nm, and $\alpha_p = 200$ μm^{-1}.

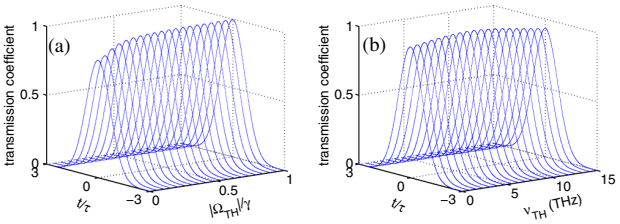

Fig. 6. (a) Surface plot of probe transmission spectra as a function of the dimensionless time t/τ and amplitude $|\Omega_{TH}|$ with $\Delta_{TH} = 0$. (b) Surface plot of probe transmission spectra as a function of the dimensionless time t/τ and the THz signal frequency with $|\Omega_{TH}| = \gamma$. Other parameters are $B = 3T$, $\tau = 1$ ps, $\Delta_p = 0$, $\gamma = 3 \times 10^{13}$ s^{-1}, $\gamma_3 = \gamma$, $\gamma_2 = 0.05\gamma$, $|\Omega_p| = 0.05\gamma$, $L = 0.4$ nm, and $\alpha_p = 200$ μm^{-1}.

the results of Figs. 5(a) and 5(b) illustrates that the transparency window can be obviously enlarged with the amplitude $|\Omega_{TH}|$ increasing.

Up to now, we have demonstrated that the THz signal detection scheme can be achieved in the present graphene under the external magnetic field based on quantum interference theory. Since the probe and THz signal fields are in the form of optics pulses, we also consider how to simulate a practical approach. Thus, we assume that a weak Gaussian-shaped probe light (i.e., $\Omega_p^{\text{in}} = e^{-t^2/\tau^2}$) with the pulse width $\tau = 1$ ps passes through the magnetized graphene structure. Now, the transmitted probe field can be rewritten as $\Omega_p^{\text{out}} = e^{-t^2/\tau^2} e^{-\alpha_p L \gamma_3 \text{Im}(\frac{\rho_{31}}{\Omega_p})}$. In Fig. 6, we show the results from numerical simulations with the different cases. For one case, in Fig. 6(a), it can be clearly seen that the transmissivity of the probe field significantly decreases with the amplitude of the THz signal field increasing until the appearance of a perfect EIT transparency window, which has been introduced in Fig. 4(a). For the other case, Fig. 6(b) describes that probe transmission spectra as a function of the dimensionless time t/τ and the THz signal frequency. When the magnetic field remains fixed, the transparency window can be opened under the resonance condition of the signal field (i.e., the THz signal frequency equals the transition frequency between states $|2\rangle$ and $|3\rangle$). These observations are indeed similar to the previous research and prove the feasibility of this scheme. Specifically, similar to our Λ-type model, the V- and cascade-type schemes based on the three-state EIT can be suggested for detecting THz signal in a graphene system.

4. CONCLUSION

In conclusion, we have performed a scheme to realize THz signal detection under an external magnetic field due to the strong optical response of a graphene system in the IR and THz region. With the aid of the EIT and quantum destructive interference, the behaviors of the probe transmission spectra are determined by switching on/off THz signal radiation. Taking this theory and solving the coupled Schrödinger–Maxwell formula, we demonstrate that the magnetized graphene provides the EIT transparency window in the presence of the THz signal field, in which the probe pulse propagates with an extremely slow group velocity. Furthermore, the behavior of the probe transmission spectra can be controlled by means of the optical absorption property of the graphene system so that a broad THz signal frequency bandwidth can be accurately inspected. As a result, the above excellent performances demonstrate that the graphene has a admirable potential to utilize its optical property in the design of optical detectors.

APPENDIX A

When the magnetic field is perpendicularly applied in a single-layer graphene (in the $z-y$ plane), the effective-mass Hamiltonian [49–51] without external optical field can be written as

$$\hat{H}_0 = \upsilon_F \begin{pmatrix} 0 & \hat{\pi}_x - i\hat{\pi}_y & 0 & 0 \\ \hat{\pi}_x + i\hat{\pi}_y & 0 & 0 & 0 \\ 0 & 0 & 0 & \hat{\pi}_x + i\hat{\pi}_y \\ 0 & 0 & \hat{\pi}_x - i\hat{\pi}_y & 0 \end{pmatrix}, \tag{A1}$$

where Fermi velocity $\upsilon_F = 3\gamma_0/2\hbar a \approx 10^6$ m/s is a band parameter with the nearest-neighbor hopping energy $\gamma_0 \sim 2.8$ eV and C-C spacing $a = 1.42\mathring{A}$, $\hat{\vec{\pi}} = \hat{\vec{p}} + e\vec{A}/c$ represents the generalized momentum operator, $\hat{\vec{p}}$ is the electron momentum operator, e is the electron charge, and $\vec{A}$ is the vector potential, which is equal to $(0, Bx)$ for a uniform magnetic field. In general, one can obtain the eigenenergies of discrete LLs for the magnetized graphene by solving the effective mass Schrödinger equations, i.e., $\hat{H}_0\Psi = \varepsilon\Psi$. In fact, the Hamiltonian near the K point can be expressed as $\hat{H}_0 = \upsilon_F \hat{\vec{\sigma}} \cdot \hat{\vec{\pi}}$, where $\hat{\vec{\sigma}} = (\hat{\sigma}_x, \hat{\sigma}_y)$ is a vector of Pauli matrices. Then, the eigenfunction is specified by two quantum numbers $n(n = 0, \pm 1, \pm 2, \ldots)$ and the electron wave vector k_y along the y direction [6,10,49],

$$\Psi_{n,k_y}(r) = \frac{C_n}{\sqrt{L}} e^{(-ik_y y)} \begin{pmatrix} \text{sgn}(n) i^{|n|-1} \varphi_{|n|-1} \\ i^{|n|} \varphi_{|n|} \end{pmatrix}, \tag{A2}$$

with

$$C_n = \begin{cases} 1 (n = 0) \\ \frac{1}{\sqrt{2}} (n \neq 0) \end{cases}, \tag{A3}$$

and

$$\varphi_{|n|} = \frac{H_{|n|}((x - l_c^2 k_y)/l_c)}{\sqrt{2^{|n|}|n|!\sqrt{\pi} l_c}} e^{\left[-\frac{1}{2}\left(\frac{x - l_c^2 k_y}{l_c}\right)^2\right]}, \tag{A4}$$

where $l_c = \sqrt{c\hbar/eB}$ is magnetic length and $H_n(x)$ is the Hermite polynomial. The eigenenergy can be calculated as $\varepsilon_n = \text{sgn}(n)\hbar\omega_c\sqrt{|n|}$ with $\omega_c = \sqrt{2}\upsilon_F/l_c$. In comparison with LLs of a conventional 2D electron/hole system with a parabolic dispersion, LLs in graphene are unequally spaced and their transition energies are proportional to $\sqrt{B}$ [6,9,10,45,46]. Combining the eigenenergy of the graphene system with the selected three energy levels in Fig. 1(b), we can simplify the system Hamiltonian without optical fields as

$$\hat{H}_0 = \hbar\varepsilon_3 |3\rangle\langle 3| + \hbar\varepsilon_2 |2\rangle\langle 2| + \hbar\varepsilon_1 |1\rangle\langle 1|. \tag{A5}$$

Considering the light–matter interaction in the graphene system, the vector potential of the optical field $\vec{A}_{\text{opt}} = ic\vec{E}/\omega$

$(\vec{E} = \vec{E}_p + \vec{E}_{TH})$ is employed in the vector potential of the magnetic field in the generalized momentum operator $\vec{\pi}$ in the Hamiltonian. The generated interaction Hamiltonian contained magnetized graphene and incident optical field can be obtained in the following form:

$$\hat{H}_{\text{int}} = v_F \vec{\sigma} \cdot \frac{e}{c} \vec{A}_{\text{opt}}. \tag{A6}$$

From the above equation, the interaction Hamiltonian does not include the momentum operator, and it is only determined by the Pauli matrix vector and proportional to vector potential $\vec{A}_{\text{opt}}$. In addition, we insert the complete set of states $\{|3\rangle, |2\rangle, |1\rangle\}$ in the generated interaction Hamiltonian. Hence we obtain

$$\begin{aligned}\hat{H}_{\text{int}} &= I \cdot v_F \vec{\sigma} \cdot \frac{e}{c} \vec{A}_{\text{opt}} \cdot I \\ &= -\mu_{31} E_p^- e^{-i\omega_p t} |3\rangle\langle 1| - \mu_{32} E_{TH}^- e^{-i\omega_{TH} t} |3\rangle\langle 2| + \text{h.c.} \\ &= -\hbar\Omega_p e^{-i\omega_p t} |3\rangle\langle 1| - \hbar\Omega_{TH} e^{-i\omega_{TH} t} |3\rangle\langle 2| + \text{h.c.},\end{aligned} \tag{A7}$$

where the complete set of states is $I = \sum_i |i\rangle\langle i|$ $(i = 1, 2, 3)$ and $\vec{\mu}_{mn} = \langle m|\vec{\mu}|n\rangle = e \cdot \langle m|\vec{r}|n\rangle = \frac{i\hbar e}{\varepsilon_n - \varepsilon_m} \langle m|v_F \vec{\sigma}|n\rangle$ denotes the dipole moments for the transition between states $|m\rangle \leftrightarrow |n\rangle$. The corresponding Rabi frequencies for the relevant laser-driven intersubband transitions are represented as $\Omega_p = (\vec{\mu}_{31} \cdot \vec{e}_-) E_p^-/\hbar$ and $\Omega_{TH} = (\vec{\mu}_{32} \cdot \vec{e}_-) E_{TH}^-/\hbar$.

Then we can get the total Hamiltonian of the graphene system, i.e., $\hat{H} = \hat{H}_0 + \hat{H}_{\text{int}}$. To simplify this formula, we assume that the state $|1\rangle$ is the zero potential reference. In the interaction picture, with the rotating wave approximation and the electric dipole approximation, the total Hamiltonian can be expressed as $(\hbar = 1)$

$$\begin{aligned}\hat{H}_{\text{int}}^I = {} & \Delta_p |3\rangle\langle 3| + (\Delta_p - \Delta_{TH}) |2\rangle\langle 2| \\ & - (\Omega_p |3\rangle\langle 1| + \Omega_{TH} |3\rangle\langle 2| + \text{h.c.}),\end{aligned} \tag{A8}$$

with the corresponding frequency detunings $\Delta_p = (\varepsilon_{n=2} - \varepsilon_{n=-1})/\hbar - \omega_p$ and $\Delta_{TH} = (\varepsilon_{n=2} - \varepsilon_{n=1})/\hbar - \omega_{TH}$.

Funding. National Natural Science Foundation of China (NSFC) (11374050, 61372102); Fundamental Research Funds for the Central Universities (2242012R30011); Scientific Research Foundation of Graduate School of Southeast University (YBJJ1522).

REFERENCES

1. R. R. Nair, P. Blake, A. N. Grigorenko, K. S. Novoselov, T. J. Booth, T. Stauber, N. M. R. Peres, and A. K. Geim, "Fine structure constant defines visual transparency of graphene," Science **320**, 1308 (2008).
2. A. H. Castro Neto, F. Guinea, N. M. R. Peres, K. S. Novoselov, and A. K. Geim, "The electronic properties of graphene," Rev. Mod. Phys. **81**, 109–162 (2009).
3. M. Yankowitz, J. Xue, D. Cormode, J. D. Sanchez-Yamagishi, K. Watanabe, T. Taniguchi, P. Jarillo-Herrero, P. Jacquod, and B. J. LeRoy, "Emergence of superlattice Dirac points in graphene on hexagonal boron nitride," Nat. Phys. **8**, 382–386 (2012).
4. M. L. Sadowski, G. Martinez, M. Potemski, C. Berger, and W. A. de Heer, "Landau level spectroscopy of ultrathin graphite layers," Phys. Rev. Lett. **97**, 266405 (2006).
5. D. S. L. Abergel and V. I. Fal'ko, "Optical and magneto-optical far-infrared properties of bilayer graphene," Phys. Rev. B **75**, 155430 (2007).
6. X. Yao and A. Belyanin, "Giant optical nonlinearity of graphene in a strong magnetic field," Phys. Rev. Lett. **108**, 255503 (2012).
7. L. G. Booshehri, C. H. Mielke, D. G. Rickel, S. A. Crooker, Q. Zhang, L. Ren, E. H. Haroz, A. Rustagi, C. J. Stanton, Z. Jin, Z. Sun, Z. Yan, J. M. Tour, and J. Kono, "Circular polarization dependent cyclotron resonance in large-area graphene in ultrahigh magnetic fields," Phys. Rev. B **85**, 205407 (2012).
8. S. H. Asadpour, H. R. Hamedi, and H. R. Soleimani, "Role of incoherent pumping field on absorption-dispersion properties of probe pulse in a graphene nanostructure under external magnetic field," Phys. E **71**, 123–129 (2015).
9. M. Tokman, X. Yao, and A. Belyanin, "Generation of entangled photons in graphene in a strong magnetic field," Phys. Rev. Lett. **110**, 077404 (2013).
10. X. Yao and A. Belyanin, "Nonlinear optics of graphene in a strong magnetic field," J. Phys. **25**, 054203 (2013).
11. K. L. Ishikawa, "Nonlinear optical response of graphene in time domain," Phys. Rev. B **82**, 201402 (2010).
12. A. R. Wright, X. G. Xu, J. C. Cao, and C. Zhang, "Strong nonlinear optical response of graphene in the terahertz regime," Appl. Phys. Lett. **95**, 072101 (2009).
13. S. A. Mikhailov and K. Ziegler, "Nonlinear electromagnetic response of graphene: frequency multiplication and the self-consistent-field effects," J. Phys. **20**, 384204 (2008).
14. T. Gu, N. Petrone, J. F. McMillan, A. van der Zande, M. Yu, G. Q. Lo, D. L. Kwong, J. Hone, and C. W. Wong, "Regenerative oscillation and four-wave mixing in graphene optoelectronics," Nat. Photonics **6**, 554–559 (2012).
15. S. A. Mikhailov, "Theory of the nonlinear optical frequency mixing effect in graphene," Phys. E **44**, 924–927 (2012).
16. C. Ding, R. Yu, J. Li, X. Hao, and Y. Wu, "Matched infrared soliton pairs in graphene under Landau quantization via four-wave mixing," Phys. Rev. A **90**, 043819 (2014).
17. C. Ding, R. Yu, J. Li, X. Hao, and Y. Wu, "Formation and ultraslow propagation of infrared solitons in graphene under an external magnetic field," J. Appl. Phys. **115**, 234301 (2014).
18. S. E. Harris and L. V. Hau, "Nonlinear optics at low light levels," Phys. Rev. Lett. **82**, 4611–4614 (1999).
19. M. Fleischhauer, A. Imamoglu, and J. P. Marangos, "Electromagnetically induced transparency: optics in coherent media," Rev. Mod. Phys. **77**, 633–673 (2005).
20. M. Phillips and H. Wang, "Spin coherence and electromagnetically induced transparency via exciton correlations," Phys. Rev. Lett. **89**, 186401 (2002).
21. M. C. Phillips, H. Wang, I. Rumyantsev, N. H. Kwong, R. Takayama, and R. Binder, "Electromagnetically induced transparency in semiconductors via biexciton coherence," Phys. Rev. Lett. **91**, 183602 (2003).
22. M. O. Scully and M. S. Zubairy, *Quantum Optics* (Cambridge University, 1997), Chap. 7.
23. L. V. Hau, S. E. Harris, Z. Dutton, and C. H. Behroozi, "Light speed reduction to 17 metres per second in an ultracold atomic gas," Nature **397**, 594–598 (1999).
24. L. J. Wang, A. Kuzmich, and A. Dogariu, "Gain-assisted superluminal light propagation," Nature **406**, 277–279 (2000).
25. W. X. Yang, J. M. Hou, and R. K. Lee, "Ultraslow bright and dark solitons in semiconductor quantum wells," Phys. Rev. A **77**, 033838 (2008).
26. W. X. Yang, J. M. Hou, Y. Y. Lin, and R. K. Lee, "Detuning management of optical solitons in coupled quantum wells," Phys. Rev. A **79**, 033825 (2009).
27. W. X. Yang, J. M. Hou, and R. K. Lee, "Highly efficient four-wave mixing via intersubband transitions in InGaAs/AlAs coupled double quantum well structures," J. Mod. Opt. **56**, 716–721 (2009).
28. X. Hao, J. Li, and X. Yang, "Mid-infrared efficient generation by resonant four-wave mixing in a three-coupled-quantum-well nanostructure," Opt. Commun. **282**, 3339–3344 (2009).
29. Y. Wu and X. Yang, "Fully quantized theory of four-wave mixing with bosonic matter waves," Opt. Lett. **30**, 311–313 (2005).
30. A. Joshi and M. Xiao, "Optical multistability in three-level atoms inside an optical ring cavity," Phys. Rev. Lett. **91**, 143904 (2003).

31. J. Li, R. Yu, X. Hao, A. Zheng, and X. Yang, "Coherent laser-induced optical behaviors in three-coupled-quantum wells and their application to terahertz signal detection," Opt. Commun. **282**, 4384–4389 (2009).
32. S. H. Asadpour, Z. Golsanamlou, and H. R. Soleimani, "Infrared and terahertz signal detection in a quantum dot nanostructure," Phys. E **54**, 45–52 (2013).
33. H. C. Liu, C. Y. Song, A. J. SpringThorpe, and J. C. Cao, "Terahertz quantum-well photodetector," Appl. Phys. Lett. **84**, 4068–4070 (2004).
34. D. Suzuki, S. Oda, and Y. Kawano, "GaAs/AlGaAs field-effect transistor for tunable terahertz detection and spectroscopy with built-in signal modulation," Appl. Phys. Lett. **102**, 122102 (2013).
35. J. Y. Jia, J. H. Gao, M. R. Hao, T. M. Wang, W. Z. Shen, Y. H. Zhang, J. C. Cao, X. G. Guo, and H. Schneider, "Dark current mechanism of terahertz quantum-well photodetectors," J. Appl. Phys. **116**, 154501 (2014).
36. B. Ferguson and X. C. Zhang, "Materials for terahertz science and technology," Nat. Mater. **1**, 26–33 (2002).
37. M. Tonouchi, "Cutting-edge terahertz technology," Nat. Photonics **1**, 97–105 (2007).
38. T. Kiwa, J. Kondo, S. Oka, I. Kawayama, H. Yamada, M. Tonouchi, and K. Tsukada, "Chemical sensing plate with a laser-terahertz monitoring system," Appl. Opt. **47**, 3324–3327 (2008).
39. P. H. Siegel, "Terahertz technology," IEEE Trans. Microwave Theory Tech. **50**, 910–928 (2002).
40. A. V. Raisanen, "Frequency multipliers for millimeter and submillimeter wavelengths," Proc. IEEE **80**, 1842–1852 (1992).
41. Z. Jiang, E. A. Henriksen, L. C. Tung, Y. J. Wang, M. E. Schwartz, M. Y. Han, P. Kim, and H. L. Stormer, "Infrared spectroscopy of Landau levels of graphene," Phys. Rev. Lett. **98**, 197403 (2007).
42. J. Cheh and H. Zhao, "Solitons in graphene," arXiv preprint arXiv:1107.3696 (2011).
43. M. L. Nesterov, J. Bravo-Abad, A. Y. Nikitin, F. J. Garcia-Vidal, and L. Martin-Moreno, "Graphene supports the propagation of subwavelength optical solitons," Laser Photonics Rev. **7**, L7–L11 (2013).
44. H. Dong, C. Conti, A. Marini, and F. Biancalana, "Terahertz relativistic spatial solitons in doped graphene metamaterials," J. Phys. B **46**, 155401 (2013).
45. X. Yao, M. Tokman, and A. Belyanin, "Efficient nonlinear generation of THz plasmons in graphene and topological insulators," Phys. Rev. Lett. **112**, 055501 (2014).
46. X. Yao and A. Belyanin, "Giant optical nonlinearity of graphene in a magnetic field," Proc. SPIE **8604**, 860412 (2013).
47. Y. Wu and X. Yang, "Electromagnetically induced transparency in V-, Λ-, and cascade-type schemes beyond steady-state analysis," Phys. Rev. A **71**, 053806 (2005).
48. M. D. Lukin and A. Imamoglu, "Controlling photons using electromagnetically induced transparency," Nature **413**, 273–276 (2001).
49. Y. Zheng and T. Ando, "Hall conductivity of a two-dimensional graphite system," Phys. Rev. B **65**, 245420 (2002).
50. T. Ando, "Theory of electronic states and transport in carbon nanotubes," J. Phys. Soc. Jpn. **74**, 777–817 (2005).
51. T. Ando, "Magnetic oscillation of optical phonon in graphene," J. Phys. Soc. Jpn. **76**, 024712 (2007).